(4)

David Taylor Research Center

Bethesda, MD 20084-5000

DTRC/SHD-1298-06 January 1990

Ship Hydromechanics Department

Departmental Report

PRESSURE AND SHEAR STRESS MEASUREMENT UNCERTAINTY FOR DARPA SUBOFF EXPERIMENT

by

Scott Gowing

Approved for public release;
Distribution is unlimited.

DTRC/SHD-1298-06 PRESSURE AND SHEAR STRESS MEASUREMENT UNCERTAINTY FOR DARPA SUBOFF EXPERIMENT

MAJOR DTRC TECHNICAL COMPONENTS

CODE 011 DIRECTOR OF TECHNOLOGY, PLANS AND ASSESSMENT

12 SHIP SYSTEMS INTEGRATION DEPARTMENT

14 SHIP ELECTROMAGNETIC SIGNATURES DEPARTMENT

15 SHIP HYDROMECHANICS DEPARTMENT

16 AVIATION DEPARTMENT

17 SHIP STRUCTURES AND PROTECTION DEPARTMENT

18 COMPUTATION, MATHEMATICS & LOGISTICS DEPARTMENT

19 SHIP ACOUSTICS DEPARTMENT

27 PROPULSION AND AUXILIARY SYSTEMS DEPARTMENT

28 SHIP MATERIALS ENGINEERING DEPARTMENT

DTRC ISSUES THREE TYPES OF REPORTS:

1. **DTRC reports, a formal series,** contain information of permanent technical value. They carry a consecutive numerical identification regardless of their classification or the originating department.

2. **Departmental reports, a semiformal series,** contain information of a preliminary, temporary, or proprietary nature or of limited interest or significance. They carry a departmental alphanumerical identification.

3. **Technical memoranda, an informal series,** contain technical documentation of limited use and interest. They are primarily working papers intended for internal use. They carry an identifying number which indicates their type and the numerical code of the originating department. Any distribution outside DTRC must be approved by the head of the originating department on a case-by-case basis.

NDW-DTNSRDC 5602/51 (Rev 2-88)

UNCLASSIFIED
SECURITY CLASSIFICATION OF THIS PAGE

REPORT DOCUMENTATION PAGE

1a. REPORT SECURITY CLASSIFICATION Unclassified	1b. RESTRICTIVE MARKINGS
2a. SECURITY CLASSIFICATION	3. DISTRIBUTION / AVAILABILITY OF REPORT Approved for public release; distribution is unlimited.
2b. DECLASSIFICATION / DOWNGRADING SCHEDULE	
4. PERFORMING ORGANIZATION REPORT NUMBER(S) DTRC/SHD-1298-06	5. MONITORING ORGANIZATION REPORT NUMBER(S)
6a. NAME OF PERFORMING ORGANIZATION David Taylor Research Center 6b. OFFICE SYMBOL (If applicable) Code 1542	7a. NAME OF MONITORING ORGANIZATION
6c. ADDRESS (City, State, and Zip Code) Bethesda, MD 20084-5000	7b. ADDRESS (City, State, and Zip Code)
8a. NAME OF FUNDING / SPONSORING ORGANIZATION 8b. OFFICE SYMBOL (If applicable)	9. PROCUREMENT INSTRUMENT IDENTIFICATION
8c. ADDRESS (City, State, and Zip Code)	10. SOURCE OF FUNDING PROGRAM ELEMENT NO. 63569N; PROJECT NO.; TASK NO. S1974030; WORK UNIT ACCESSION NO. DN509067
11. TITLE (Include Security Classification) **PRESSURE AND SHEAR STRESS MEASUREMENT UNCERTAINTY FOR DARPA SUBOFF EXPERIMENT**	
12. PERSONAL AUTHOR(S) Scott Gowing	
13a. TYPE OF REPORT Departmental 13b. TIME COVERED FROM_____ TO_____	14. DATE OF REPORT (Year, Month, Day) 1990, January 15. PAGE COUNT 27
16. SUPPLEMENTARY NOTATION	
17. COSATI CODES FIELD / GROUP / SUB-GROUP	18. SUBJECT TERMS (Continue on reverse if necessary and identify by block number) DARPA SUBOFF, pressure measurement, shear stress, pressure distribution, obstacle block

19. ABSTRACT (Continue on reverse if necessary and identify by block number)

An uncertainty analysis of the pressure and shear stress measurements in the SUBOFF experiments is presented. Error sources in the measurements are identified, characterized as to the types of error that will result, and then quantified.

The propagation of errors in the pressure and friction coefficients is approximated with a Taylor series and the 95% confidence intervals for Cp and Cf are presented as a function of the coefficients themselves and thermal drift in the electronics. It is concluded that the true value of the pressure coefficient is within 0.005 to 0.01 of the measured value, and the true friction coefficient is within 0.0002 of its measured value.

20. DISTRIBUTION / AVAILABILITY OF ABSTRACT ☒ UNCLASSIFIED/UNLIMITED ☐ SAME AS RPT ☐ DTIC USERS	21. ABSTRACT SECURITY CLASSIFICATION Unclassified
22a. NAME OF RESPONSIBLE INDIVIDUAL Scott Gowing	22b. TELEPHONE (Include Area Code) 301-227-1410 22c. OFFICE SYMBOL Code 1542

DD FORM 1473, 84 MAR — 83 APR edition may be used until exhausted. All other editions are obsolete.

SECURITY CLASSIFICATION OF THIS PAGE

UNCLASSIFIED

CONTENTS

TABLES

FIGURES

FIGURES (continued)

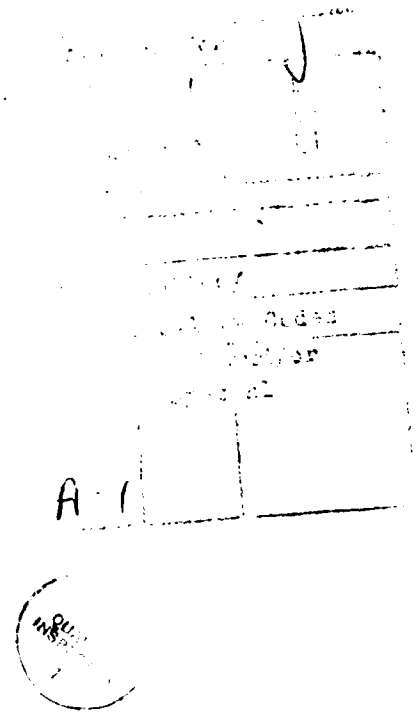

ABSTRACT

An uncertainty analysis of the pressure and shear stress measurements in the SUBOFF experiments is presented. Error sources in the measurements are identified, characterized as to the types of error that will result, and then quantified.

The propagation of errors in the pressure and friction coefficients is approximated with a Taylor series and the 95% confidence intervals for C_p and C_f are presented as a function of the coefficients themselves and thermal drift in the electronics. It is concluded that the true value of the pressure coefficient is within 0.005 to 0.01 of the measured value, and the true friction coefficient is within 0.0002 of its measured value.

ADMINISTRATIVE INFORMATION

This research was supported under the Defense Advanced Research Projects Agency (DARPA) sponsored SUBOFF experiment, Task Area S1974-030, program element 63569N, internal David Taylor Research Center (DTRC) work unit number 1-1542-123.

INTRODUCTION

This report gives an analysis of the uncertainty of the pressure and shear stress measuring systems used in the DARPA-sponsored SUBOFF experimental program. The pressure system measures pressures at 130 to 180 taps installed on an axisymmetric body and its appendages while the model is tested in a wind tunnel. The measured pressures are differential relative to the freestream static pressure and these values are normalized by dynamic pressure to yield pressure coefficients. After discussing the pressure measuring system itself, an uncertainty analysis is presented that determines the 95% confidence interval for the non-dimensional pressure coefficient.

Shear stresses are measured using the same pressure system combined with obstacle blocks that stagnate the velocity fields near the model surface. The resultant pressure rises determine the friction coefficients.

PRESSURE MEASURING SYSTEM

The heart of the pressure measuring system is a set of five rotary pressure scanners, each one tubulated to 48 pressure taps on one side and connected to its own transducer on the other. The scanners are Scanivalve Model 48J9GM modules connected to a solenoid

drive. The volume between the transducer diaphragm and the rotor mating face is very small to allow rapid scanning of the pressure taps. The transducers have four arm bridged silicon diaphragms with a full scale differential pressure range of 18 torr. Connected to each transducer's scanner are: reference pressure for a zero-differential pressure check; dynamic pressure from two pitot tubes in the tunnel freestream for normalizing pressures into pressure coefficients; and calibration pressure which connects to an independent, high accuracy pressure transducer for in situ calibration. The calibration transducer is a Datametrics Type 570 Barocel sensor with a differential pressure range of 10 torr. Connected to the transducers are Vishay Model 2310 signal conditioners that provide excitation voltage, output signal amplification, and bridge balancing. The pressure transducer used for calibration is a capacitance type with temperature control for improved thermal stability. This entire system is located in the model itself.

The scanner transducer and calibration transducer signals and the position signal from the pressure scanner system all connect to the data collection computer (MASSCOMP MC5450 Scientific Laboratory System) in the tunnel control room through a bank of Ectron Model 750 low pass filters. The filters are a 3 pole Bessel type that attenuate –3 dB at the upper cutoff frequency which was 10 KHz during the tests. Visual examination of the transducer signals on the oscilloscope showed little signal change when the cutoff frequency was lowered to 100 Hz, but the upper limit of 10 KHz was used to capture the step response of the transducers during scanning and eliminated higher frequency noise. Control lines for the scanning system and a pneumatic line for controlling calibration pressure also pass from the model into the tunnel control room. A schematic of the electronics is shown in Figure 1.

The computer samples the data from the five transducers at 1 KHz for 100 ms for each tap. The computer routine for analyzing the data divides the differential pressure measured by a transducer for a particular tap by the average dynamic pressure of the two pitot tubes measured by that same transducer. The reference pressure on the transducers is the average of the freestream static pressures from the pitot tubes, hence the computed result is the pressure coefficient for that tap.

The procedure for using the system plays a role in its accuracy. First, the wind tunnel is brought up to test speed to equalize conditions and especially to allow the air to heat up from friction. Once the tunnel temperature has stabilized the transducers are calibrated by varying the calibration pressure from the control room. Then, the tests are performed. With time, the tunnel, and consequently the model, change temperature and

the pressure system electronics experience thermal drift. The amount of drift is checked by monitoring the system with the scanners connected to the calibration pressure port. If the drift is significant, the calibration and scanner transducer readouts differ, and the system is recalibrated at the new elevated temperature.

The significant features of the pressure system are the ability for remote calibration at in situ temperature, measurement of tap and dynamic pressure with the same transducer, and high scanning speeds to survey all pressures at constant tunnel conditions.

In the following analysis, all the settings or values mentioned for the system are the same as those used in testing.

PRESSURE UNCERTAINTY ANALYSIS

The following analysis uses an approach similar to that of Abernathy, et al [1]. (References are presented on page 27.) First, all possible sources of error are identified for the pressure measuring system from the point of pressure application at the tap to the final pressure coefficient C_p. Some possible error sources can be eliminated by checking and testing of the system, others cannot be eliminated and will contribute to bias and precision type errors in the final results. These error sources are quantified and then combined in the the final calculation to yield the 95% confidence interval that contains the true value of C_p.

The desired result of the pressure system is the non-dimensional coefficient

$$C_p = \frac{P-P_s}{\frac{\rho}{2}V^2} = \frac{P-P_s}{P_T-P_S} \tag{1}$$

for which

C_p = pressure coefficient
P = local pressure on tap
P_S = freestream static pressure
P_T = freestream total pressure
V = freestream velocity
ρ = density.

ERROR SOURCES

Errors in C_p arise from errors made in measuring the numerator, $(P-P_S)$, or the denominator, (P_T-P_S). Both of these are measured directly by the transducer because the transducer's reference pressure is the freestream static pressure. The following list details all the possible error sources in the measurement of the quantities $P-P_S$ or P_T-P_S:

1. burrs on the pressure taps
2. tap holes not normal to surface
3. leaks in tap to tubing and tubing to pressure scanner connections
4. insufficient time during pressure scanning for pressure equalization between tap and transducer cavity
5. insufficient frequency response of signal conditioning to step changes in pressure
6. mechanical binding of transducer diaphragm from improper construction or installation
7. leakage between scanner rotor and mating face assembly
8. bias and precision errors in calibration transducer relative to NIST (National Institute for Standards and Technology) values.
9. thermal drift of zero point and sensitivity in calibration transducer.
10. nonlinearity of scanner transducer output
11. statistical (precision) errors in computer routine for calibration of scanner transducers
12. thermal drift of zero point and sensitivity in scanner pressure transducer
13. thermal drift in excitation voltage
14. thermal drift in amplifier gain
15. resolution limits of bridge balance circuit on scanner transducers
16. noise in excitation voltage, bridge balance, amplifier, filter, and A/D convertor circuits
17. thermal drift in filter circuit gains
18. thermal drift of A/D converter gain
19. resolution limits of A/D converter
20. bias error in A/D converter circuit
21. pitot tube misalignment

Numerical resolution and truncation errors in the computer are assumed to be negligible. The size of the tap hole, 1/32 in (.079 cm), is assumed to cause negligible errors.

The calibration of the scanner transducers measures the output of the transducers through the signal conditioners, amplifiers, filters and A/D converter, against the voltage output of the calibration transducer measured through the A/D convertor. Thus, bias errors and non-linearities in the scanner transducer sensitivities, excitation voltage settings, amplifier gain settings, and filter gain settings and A/D converter are all internal to the calibration procedure. Bias errors in the A/D convertor are not negligible in the calibration signal channel because bias errors there will affect the calibration transducer output. Pitot tube errors are assumed to be negligible for perfect alignment with the flow, and temperature measurement errors are assumed to be negligible when calculating thermal drift errors in the electronics.

ERROR ESTIMATES

The following table lists values for the bias and precision errors that arise from each source, or checks and remedies that were applied to the error source to nullify it. Most of the values were taken from company literature. All errors are listed in torrs, the unit of pressure used in the test program. Note that some errors are not symmetric and some are proportional to reading (differential pressure on the transducer). In the latter case, the error is expressed as a function of pressure coefficient, hence the accuracy of the pressure coefficient becomes dependent on the coefficient's magnitude. Each bias error is denoted with a "b" and subscripted with the number of the error source that causes it, and precision errors are denoted with "s" and similarly subscripted. Because the error may depend on the magnitude of the reading, those errors will be different for the numerator value (P_T-P_S) than for the denominator value (P_T-P_S) in C_p.

TABLE 1. Error sources and values in pressure measurements.

Error Source #	Remedy or Error Type and Value
1.	The taps were inspected for burrs. None were found.
2.	A drill bit was inserted into the taps. Minor deviations from normal were noted, but they were assumed to cause negligible errors.
3.	The taps were plugged from the outside and pressurized through the scanner with a small, closed volume of high pressure gas. No leaks were found.

TABLE 1. (cont'd) Error sources and values in pressure measurements.

Error Source #	Remedy or Error Type and Value

4. The pressure signal was monitored with an oscilloscope while the scanner stepped from a tap with zero differential pressure to a tap connected through a long tube to full dynamic pressure. Pressure equalization occurred in two to five milliseconds. The scanner stepping rate during testing is 0.5 Hz with data collection occurring in the last 190 ms of tap connection. This rate allows full pressure equalization.

5. No ringing or overshoot in the pressure signal was noted during the test described above, hence the system frequency response is adequately high.

6. Binding of the transducer diaphragm will appear as a severe nonlinearity on a calibration curve. All the curves appeared sufficiently linear that this error source could not have occurred.

7. Data from the pressure scanner company indicate a nominal leakage rate equivalent to a 0.5 in Hg pressure rise in 5 cm^3 at 24 in Hg vacuum. This leakage will produce a bias opposite in sign to C_p and proportional to C_p. The bias error will be assumed to be symmetric because the values of C_p are both positive and negative in the testing
$b_7 = \pm 8.48 \times 10^{-5} (C_p)$ torr.

8. The calibration system (transducer and readout) accuracy is listed as 0.08% of reading traceable to NIST. Assume that this error is all bias type. The bias error is then estimated as the average bias that would occur over a calibration range of ±9 torr. This is the range of pressures that occurred in testing.
$b_8 = \pm 3.60 \times 10^{-3}$ torr

9. The calibration transducer is mounted on a temperature control base to minimize thermal fluctuations in the reading. The base heats the transducer to 40°C to allow temperature control by heating alone. The temperature in the base still varies ±1.7°C of the set point. Assuming this variation is normally distributed, the transducer will experience a precision error. Assume the limits of the temperature excursions are 2σ of the fluctuations, then 1σ on temperature is 0.85°C. The temperature coefficients of the transducer are ±0.003% FS/°C on zero and 0.03%/°C on sensitivity. This results in a precision error dependent on reading. Assume an average reading during calibration of ±4.5 torr, because the calibration pressures ranged from –9 to +9 torr.
$s_9 = 2.55 \times 10^{-4}$ torr + 1.15×10^{-3} torr
$= 1.4 \times 10^{-3}$ torr

TABLE 1. (cont'd) Error sources and values in pressure measurements.

Error Source #	Remedy or Error Type and Value

10. Non-linearities yield bias errors between the calibration curve fit of the scanner transducer output and the calibrating transducer output at the same pressure. The root mean square (rms) deviation of the curve-fitted transducer output from calibration value over a 20 point calibration was 5.91×10^{-3} torr for the worst transducer. This value is used to estimate non-linearity bias.
$b_{10} = \pm 5.91 \times 10^{-3}$ torr (Note: The rms deviations did not depend on range.)

11. During a calibration of the scanner transducers the computer sampled the transducer output 5000 times at each point. These samples had a typical standard deviation of $\pm$ 2.56×10^{-3} torr at each point. This value is used to estimate scanner transducer precision error with constant input pressure. This precision error did not vary with reading.
$s_{11} = 2.56 \times 10^{-3}$ torr

12. Temperature variations in the wind tunnel will change the temperature of the electronics in the model. Bias errors of unknown sign will then occur if the test temperature varies form the temperature at calibration. Temperature coefficients of the scanner transducers are $\pm 0.05\%$ FS/°C on zero and $\pm 0.02\%$/°C on sensitivity.
$b_{12} = \pm[9.00 \times 10^{-3}$ torr $+ \pm 1.73 \times 10^{-3}$ (C_p) torr$]$/°C

13. Excitation voltage thermal stability is listed as $\pm 0.01\%$/°C. This produces an unknown bias error.
$b_{13} = \pm 8.66 \times 10^{-4}$ (C_p) torr/°C

14. Amplifier output drift is listed as $\pm 2\mu$V/°C referred to input at x100 gain. The gain in the system is x800. This yields an equivalent drift in pressure that is calculated by the calibration constant of torr/volt.
$b_{14} = \pm 1.60 \times 10^{-5}$ torr/°C

15. Bridge balance resolution will show up in the signal as bias error of unknown sign. The resolution is 1.2×10^{-6} volts/volt excitation. 12VDC excitation was used in testing.
$b_{15} = \pm 1.35 \times 10^{-5}$ torr

16. Noise in the circuits from the excitation voltage circuit to the A/D convertor circuit was measured by looking at scatter in the scanner transducer signals with constant input pressure. This precision error enters into the analysis

TABLE 1. (cont'd) Error sources and values in pressure measurements.

Error Source #	Remedy or Error Type and Value

twice because it affects both the precision of the calibration routine and the data collection routine independently. This is because the number of samples collected in these routines are not necessarily the same.

$s_{16} = 2.56 \times 10^{-3}$ torr

17. The filter and A/D circuits are in the tunnel control room where temperature excursions are not as great as in the tunnel. The temperature changes in the room will produce some minor bias errors. For the filters, the specifications are ±0.003%/C on gain.

$b_{17} = \pm 2.60 \times 10^{-4} (C_p)$ torr/°C

18. Specifications for thermal stability in the A/D convertor gain circuit show ±0.005% /°C.

$b_{18} = \pm 4.33 \times 10^{-4}$ torr (C_p) torr /°C

19. Resolution limits in the A/D convertor yield bias errors of unknown sign in the result. With the gain settings used, this resolution limit was ±1 bit or ±0.00488 volts.

$b_{19} = \pm 4.58 \times 10^{-3}$torr

20. Errors in the A/D convertor gain accuracy produce bias errors of the calibration transducer signal going into the computer. Accuracy is listed as ±0.1% typical. Assume a nominal calibration reading of ±4.5 torr as before.

$b_{20} = \pm 4.50 \times 10^{-3}$ torr

21. Pitot tube misalignment causes errors in both the freestream static pressure and the dynamic pressure measurements. The tube was aligned as closely as possible by sighting which is assumed to be within ±3° of the flow. For this error in alignment, company data indicate a negative bias error in static pressure equal to -0.5% of dynamic pressure. The dynamic pressure bias error is +0.4%. For a constant dynamic pressure of 8.66 torr, these biases become one-sided constants.

$b_{21} = +4.33 \times 10^{-2}$ torr for $P\text{-}P_S$ measurements

$b_{21} = +3.46 \times 10^{-2}$ torr for $P_T\text{-}P_S$ measurements

Before proceeding to the uncertainty calculation, the degrees of freedom must be established for each precision error. This is because the confidence interval for any measurement depends not only on the precision error of the measurement, but also on how many times the measurement is taken. Thirty or more measurements will reduce the uncertainty interval to approximately the minimum that may be realized. The following table lists the degrees of freedom associated with each sampling process. The degrees of freedom are typically the number of independent samples taken for a particular measurement minus one. (The time interval between computer samples is about the same as the time required for the largest boundary layer eddies to convect past the tap, thus the samples are independent.) Degrees of freedom are denoted by "df" and subscripted according to their error source.

TABLE 2. Error sources and degrees of freedom in pressure measurements.

Error Source #	Degrees of Freedom
9.	Scanner transducer calibrations typically involve about 12 points. $df_9 = 11$
11.	The scanner transducers are sampled about 5000 times in the calibration routine. $df_{11} \equiv 5000$
16.	During testing each pressure tap is sampled for 190 ms at 1 KHz to produce 190 points. $df_{16} = 189$

UNCERTAINTY CALCULATIONS

The pressure coefficient C_p is the ratio of two independent measurements. The bias and precision errors for C_p can be estimated by combining the errors in the numerator and denominator measurements through a Taylor series expansion:

$$b_{C_p} = [(\frac{\partial C_p}{\partial \Delta P_x} b_x)^2 + (\frac{\partial C_p}{\partial \Delta P_d} b_d)^2]^{1/2} \quad (2)$$

$$s_{C_p} = [(\frac{\partial C_p}{\partial \Delta P_x} s_x)^2 + (\frac{\partial C_p}{\partial \Delta P_d} s_d)^2]^{1/2} \quad (3)$$

for which:

b_{C_p} = bias error for C_p

b_x = bias error for $(P-P_S)$ (torr)

b_d = bias error for (P_T-P_S) (torr)

ΔP_x = $(P-P_S)$ (torr)

ΔP_d = (P_T-P_S) = 8.66 torr during testing

s_{C_p} = precision error for C_p

s_x = precision error for $(P-P_S)$ (torr)

s_d = precision error for (P_T-P_S) (torr)

Assuming the elemental bias and precision errors are independent, the total bias or precision error for ΔP_x or ΔP_d can be root sum squared:

$$\pm b_{x,d} = [(\pm b_1^2) + (\pm b_2^2) + (\pm b_3^2) \ldots]^{1/2} \quad \text{(torr)} \tag{4}$$

$$s_{x,d} = [s_1^2 + s_2^2 + s_3^2 \ldots]^{1/2} \quad \text{(torr)} \tag{5}$$

The degrees of freedom for the measurement of C_p can be estimated by the Welch-Satterthwaite formula:

$$df_{C_p} = \frac{[(\frac{\partial C_p}{\partial \Delta P_x} s_x)^2 + (\frac{\partial C_p}{\partial \Delta P_d} s_d)^2]^2}{\frac{(\frac{\partial C_p}{\partial \Delta P_x} s_x)^4}{df_x} + \frac{(\frac{\partial C_p}{\partial \Delta P_d} s_d)^4}{df_d}} \tag{6}$$

in which:

df_{C_p} = degrees of freedom for C_p

df_x = degrees of freedom for ΔP_x

df_d = degrees of freedom for ΔP_d

and elemental degrees of freedom can similarly be summed:

$$df_{x,d} = \frac{[s_1^2 + s_2^2 + s_3^2 \ldots]^{1/2}}{\frac{s_1^4}{df_1} + \frac{s_2^4}{df_2} + \frac{s_3^4}{df_3} \cdots} \tag{7}$$

The net 95% confidence interval for the value of C_p becomes:

$$C_p + (-b_{C_p} - T_{.95}\, s_{C_p}) \quad \text{to} \quad C_p + (+b_{C_p} + T_{.95}\, s_{C_p}) \tag{8}$$

for which:

C_p = measured value of C_p

$T_{.95}$ = factor multiplied by precision error s_{C_p} to yield 95% confidence at degrees of freedom equal to df_{C_p} *(from student-T distribution)*

Now the elemental bias and precision errors listed in Table 1 and the degrees of freedom in Table 2 can be combined. Because some of the bias errors are not symmetric (b_{21}, for example), the positive and negative biases must be calculated separately. Bias or precision errors that depend on C_p retain their dependence when calculating the errors for ΔP_x, but they may be multiplied by 1.0 for calculating error in the measurement of ΔP_d because that is the pressure coefficient for dynamic pressure. The thermal drift errors are summed as functions of tunnel or control room temperature deviations from the temperature at calibration , i.e.,

ΔT_t = temperature deviation from tunnel temperature at calibration (°C)

ΔT_{cr} = temperature deviation from control room temperature during calibration (°C)

In the following calculations, bias errors whose magnitudes are on the order of 1% or less of the magnitude of other bias errors are dropped for simplicity. First, the elemental bias and precision errors are summed.

$$+b_x = \{8.91\times10^{-5} + 7.19\times10^{-9}\,(C_p)^2 + 8.10\times10^{-5}\,(\Delta T_t)^2 + 3.74\times10^{-6}\,(C_p)^2\,(\Delta T_t)^2 + 2.55\times10^{-7}\,(C_p)^2\,(\Delta T_{cr})^2 + 1.87\times10^{-3}\}^{1/2} \text{ torr}$$

$$-b_x = \{(+b_x)^2 - 1.87\times10^{-3}\}^{1/2} \text{ torr}$$

$$+b_d = \{8.91\times10^{-5} + 8.47\times10^{-5}\,(\Delta T_t)^2 + 2.55\times10^{-7}\,(\Delta T_{cr})^2 + 1.20\times10^{-3}\}^{1/2} \text{ torr}$$

$$-b_d = \{(+b_d)^2 - 1.20\times10^{-3}\}^{1/2} \text{ torr}$$

$$s_x = \{1.51\times10^{-5}\}^{1/2} = 3.88\times10^{-3} \text{ torr}$$

$$s_d = \{1.51\times10^{-5}\}^{1/2} = 3.88\times10^{-3} \text{ torr}$$

Now the magnitude of the different errors may be compared. The largest positive bias errors arise from pitot tube misalignment and thermal drift in the electronics in the

model, if the temperature rise is about 5°C or more. The thermal drift dominates the negative bias error. Grouping like terms, eliminating negligible terms, and simplifying,

$$+b_x = \{1.96\times10^{-3} + 8.10\times10^{-5}\,(\Delta T_t)^2\}^{1/2} \text{ torr}$$

$$-b_x = \{8.91\times10^{-5} + 8.10\times10^{-5}\,(\Delta T_t)^2 + 3.74\times10^{-6}\,(C_p)^2\,(\Delta T_t)^2\}^{1/2} \text{ torr}$$

$$+b_d = \{1.29\times10^{-3} + 8.47\times10^{-5}\,(\Delta T_t)^2\}^{1/2} \text{ torr}$$

$$-b_d = \{8.91\times10^{-5} + 8.47\times10^{-5}\,(\Delta T_t)^2 + 2.55\times10^{-7}\,(\Delta T_{cr})^2\}^{1/2} \text{ torr}$$

The degrees of freedom are calculated,

$$df_x = \frac{[(1.40\times10^{-3})^2 + 2(2.56\times10^{-3})^2]^2}{\frac{(1.40\times10^{-3})^4}{11} + \frac{(2.56\times10^{-3})^4}{5000} + \frac{(2.56\times10^{-3})^4}{189}}$$

$$= 388$$

$$df_d = 388 \text{ also.}$$

Now the total bias and precision errors are calculated.

$$\frac{\partial C_p}{\partial \Delta P_x} = \frac{1}{8.66} \text{ torr}^{-1} \qquad \frac{\partial C_p}{\partial \Delta P_d} = \frac{-\Delta P_x}{\Delta P_d^2} = \frac{-C_p}{8.66} \text{ torr}^{-1}$$

$$+b_{C_p} = \{(\frac{1}{8.66})^2\,[1.96\times10^{-3} + 8.10\times10^{-5}\,(\Delta T_t)^2]$$

$$+ (\frac{C_p}{8.66})^2\,[1.29\times10^{-3} + 8.47\times10^{-5}\,(\Delta T_t)^2]\}^{1/2}$$

$$-b_{C_p} = \{(\frac{1}{8.66})^2\,[8.91\times10^{-5} + 8.10\times10^{-5}\,(\Delta T_t)^2 + 3.74\times10^{-6}\,(C_p)^2\,(\Delta T_t)^2]$$

$$+ (\frac{C_p}{8.66})^2\,[8.91\times10^{-5} + 8.47\times10^{-5}\,(\Delta T_t)^2 + 2.55\times10^{-7}\,(\Delta T_{cr})^2]\}^{1/2}$$

$$s_{C_p} = \{(\frac{1}{8.66})^2\,(3.88\times10^{-3})^2 + (\frac{C_p}{8.66})^2\,[3.88\times10^{-3})^2\}^{1/2} = \{2.01\times10^{-7})\,(1+C_p^2)\}^{1/2}$$

and the degrees of freedom are

$$df = \{(\frac{3.88\text{x}10^{-3}}{8.66})^2 (1 + C_p^2)\}^2 / \{\frac{(\frac{3.88\text{x}10^{-3}}{8.66})^4}{388} (1 + C_p^4)\}$$

Because the pressure coefficients range from 0 to 1 in magnitude, the minimum value for df_{Cp} becomes:

$$df_{Cpminimum} = 388$$

and the value for $T_{.95}$ from the student-t distribution is approximately 2 [2].

The bias and precision error values are plotted in Figure 2 as a function of C_p and temperature rise in the tunnel ΔT_t. The thermal drift errors from control room temperature fluctuations are negligible. The majority of pressure coefficients measured during testing range from 0 to 0.3. Over this range, the errors that depend on C_p are approximately the same. Hence a single line on the graphs represents the average of their values. Note that the precision errors are not temperature dependent, but they are plotted on Figure 2 for visual comparison. Figure 3 shows the net uncertainty interval for C_p as a function of tunnel temperature and magnitude of C_p itself.

During testing, the dynamic pressures measured by the two pitot tubes are monitored to check their agreement. Because each pitot tube is connected to the same transducer and the tubes are similarly located in the tunnel, any difference in reading indicates misalignment of one of the tubes. The dynamic pressures typically are within 0.1% of each other, indicating that the tubes are parallel within 2° of each other, based on company data. The pitot tubes can still be misaligned to the flow, but it is doubtful that both tubes will be misaligned the same amount. To check the influence of thermal drift during testing, the pressure system is occasionally stepped to the calibration pressure port and the calibration transducer reading is compared to the scanning system transducer outputs which use the most recent calibration. If their outputs differ more than about $2\text{x}10^{-3}$ torr, the system is recalibrated at the new tunnel temperature and this reduces thermal drift induced errors.

SHEAR STRESS MEASUREMENTS

Shear stress on a body in a flow can be measured with small obstacles that stagnate the velocity field near the surface to produce a pressure rise that is approximately

proportional to shear stress [3]. This technique easily adapts to models that are already equipped with pressure taps for surveying pressure distributions. The pressure or pressure coefficient is measured at the tap with and without the obstacles, and the difference in the measurements indicates the shear stress or friction coefficient at that location.

For the SUBOFF experiment, small blocks similar to those developed by Nituch and Rainbird are used for obstacles [4] as shown in Figure 4. The block is attached on the downstream edge of the tap with silicone rubber compound and it is aligned by matching the cutout on the upstream face with the tap hole itself. The blocks are thinner than Nituch and Rainbird's specifications, being 2 tap diameters thick as opposed to 3. This change insures that the blocks will not intercept the outer edge of the boundary layer near the front of the model where the layer is thinner. Based on flat plate estimates, the blocks are less than 12% of the boundary layer thickness wherever they are used, and the top edge of the block is at a non-dimensional boundary layer height of $y^+ \cong 160$.

OBSTACLE BLOCK CALIBRATIONS

All the obstacle blocks were calibrated with Preston tubes using the calibrations published by Patel as reported in Winter [4]. The blocks were calibrated on the wall of a wind tunnel and then calibrated on the SUBOFF model surface itself. In both cases, the blocks were placed midspan between two Preston tubes two inches apart and the average stress indicated by the tubes was the calibration value. This compensated for any spanwise variation in shear stress between the block and the tubes. The two calibrations (tunnel wall and model surface) on each block were compared and there was no significant difference in them in the range of shear stress where the calibrations overlapped, as presented in Figure 5. Overall, the blocks produce a pressure rise that is about 75% of the pressure rise produced by a similar size Preston tube.

The calibration data were reduced to the power law expression:

$$\Delta P = 23.84 \left(\frac{h^2}{\rho \nu^2}\right)^{0.142} \tau_w^{1.14} \tag{9}$$

for which

ΔP = pressure increase with block
h = block thickness (height)
τ_w = shear stress
ν = kinematic viscosity

For comparison, Nituch and Rainbird's blocks that are 50% thicker have a calibration of:

$$\Delta P = 30.41 \left(\frac{h^2}{\rho v^2}\right)^{0.132} \tau_w^{1.13} \tag{10}$$

At a typical shear stress for the model of 0.022 torr, using the thinner blocks reduces the pressure rise 31% from the corresponding value for the thicker blocks. The calibration of the thin blocks can be nondimensionalized for the friction coefficient:

$$C_f = 0.06773 \, (R_{eb})^{-0.248} \, (\Delta C_p)^{0.876} \tag{11}$$

for which

C_f = friction coefficient
R_{eb} = Reynolds number based on obstacle block thickness
ΔC_p = pressure coefficient increase with block

This equation is used for deriving friction coefficients from the pressure measuring system which yields values for C_p.

BLOCK MISALIGNMENT AND PROXIMITY EFFECTS

If the obstacle block is not facing directly into the flow, the pressure rise will be different than for an aligned block.

This effect must be considered because some of the shear stress measurements are made near appendage and sail junctions where the surface flow is no longer parallel to the body. Instead of performing flow visualization, the blocks were aligned to the best estimate of the flow direction and this estimate is assumed to be within 15° of the true flow direction.

The pressure rises on the blocks were measured during calibration at flow misalignment angles up to 35° in 5° increments and the results are shown in Figure 6. Up to a misalignment of 15°, the pressure rises, and hence the friction coefficient, will be within 5% of the value that would be measured with an aligned block.

Because the SUBOFF experiment requires friction coefficients to be measured at many taps, it is desired to use as many blocks as possible at one time to minimize the required number of tunnel runs. It was decided not to place any blocks upstream of other

blocks to insure that there would be no interference in the flow direction. It was desired to place blocks close together in a spanwise direction to increase the number of blocks per run. On the wall of the wind tunnel, the pressure rise on a block was measured with a second block placed 1.4, 2, 6 and 10 block widths away to the side and the results are shown in Figure 7. No interference effects occur with block separations of 3 block widths or greater.

SHEAR STRESS UNCERTAINTY ANALYSIS

The accuracy of the shear stress measurements can be estimated by a method similar to that of Abernathy [1]. The desired result is the friction coefficient determined by

$$C_f = 0.06773\ (Re_b)^{-0.248}\ (\Delta C_p)^{0.876}$$

This equation comes from the best fit power law for the calibrations with the Preston tubes.

ERROR SOURCES

The following lists the sources of error that can lead to inaccuracies in the friction coefficient measurements:

1. Bias errors of Patel's Preston tube calibrations from true shear stress values, including the effect of pressure gradients on the Preston tube readings. This pressure gradient effect must be considered because the block calibrations done on the model surface were in a mild negative pressure gradient region.

2. Errors in calculating the block Reynolds number Re_b (pitot tube velocity errors, block height measurement errors, viscosity errors).

3. Calibration curve fit errors of the block calibrations to the Preston tube values.

4. Errors in the measured pressure coefficients.

5. Misalignment of the blocks relative to the flow.

6. Proximity effects of neighboring blocks when 2 or more blocks are used side by side.

ERROR ESTIMATES

The magnitude and sign of the above errors are now estimated.

TABLE 3. Error sources and values in shear measurements.

Error Source #	Remedy or Error Type and Value

1. Patel published accuracy estimates for his Preston tube calibrations when used in a pressure gradient. A pressure gradient parameter was calculated for the gradient measured on the model where the calibrations occurred. The parameter's value is in the range in which the Preston tube results are accurate to within 3%. This number estimates the bias error of Patel's calibration including pressure gradient effects. This error shows up in the equation for C_f in the proportionality constant and exponent derived from the calibration curve fit, 0.06773 and 0.876, respectively, since the error would be in the shear stress values themselves. Instead of propagating the error through those two terms, this error is approximated instead as a bias error of C_f itself and is considered after the propagation of the other errors is calculated.
   $b_1 = \pm 3.00 \times 10^{-2} C_f$

2. Assume cumulative errors in calculating Re_b do not exceed ±2% bias. This error source contributes negligibly to the overall error anyway as will be shown later.
   $b_2 = \pm 2.00 \times 10^{-2} \ Re_b$
   $= \pm 8.68 \times 10^{1}$ at $Re_b = 4.34 \times 10^{3}$

3. The root mean square deviation of the shear stress calculated by the calibration curve fit for the blocks from that measured by the Preston tubes was 2.52×10^{-5} torr for a typical calibration of 9 points. This approximates the bias error in the obstacle block calibrations relative to the Preston tubes. It enters into the calculation for C_f through the constant and exponent derived in the calibration curve fit, so this error is instead considered as bias in the coefficient C_f itself as in error no. 1 above.
   $b_3 = \pm 2.52 \times 10^{-4}$ torr
   $= \pm 2.91 \times 10^{-5}$ at $\rho V^2/2 = 8.66$ torr

4. From the previous accuracy analysis, bias errors in the measurement of C_p are ±0.008 on the average. The measurement of two C_p values to determine the ΔC_p makes the average bias error of ΔC_p the square root of twice the single C_p bias error.
   $b_4 = \pm \sqrt{2} \ b_{C_p}$
   $= \pm 1.13 \times 10^{-2}$

5. Misalignment of the block relative to the flow causes differences in the pressure rise or equivalent differences in ΔC_p. For misalignments of ±15° or less, the

TABLE 3. (cont'd) Error sources and values in shear measurements

Error Source #	Remedy or Error Type and Value
	pressure rise or ΔC_p changes only 5%. This error propagates to C_f through the value of ΔC_p. $b_5 = \pm 5.00 \times 10^{-2}\ \Delta C_p$
6.	All measurements with the obstacle blocks were made with spanwise separations of 4 block widths or greater, hence there was no interference effect from one block to the next.

UNCERTAINTY CALCULATIONS

The bias error for C_f is estimated by first determining the propagation of errors in Re_b and ΔC_p from sources nos. 2, 4 and 5. These errors are then combined with the errors from sources nos. 1 and 3.

$$b_{C_f} = [\, b_1^2 + b_3^2 + (\frac{\partial C_f}{\partial Re_b}\, b_{Re_b})^2 + (\frac{\partial C_f}{\partial \Delta C_p}\, b_{\Delta C_p})^2 \,]^{1/2}$$

for which

$$b_{Re_b} = b_2$$

$$b_{\Delta C_p} = (b_4^2 + b_5^2)^{1/2}$$

$$\frac{\partial C_f}{\partial Re_b} = -0.248\ Re_b^{-1}\ C_f$$

$$= -5.71 \times 10^{-5}\ Cf \quad \text{at} \quad Reb = 4.34 \times 10^3$$

$$\frac{\partial C_f}{\partial \Delta C_p} = 0.876\ \Delta C_p^{-1}\ C_f$$

$$b_{\Delta C_p} = [(\sqrt{2}\ b_{C_p})^2 + (5.00 \times 10^{-2}\ \Delta C_p)^2]^{1/2}$$

$$= (1.28\times10^{-4} + 2.50\times10^{-3}\,\Delta Cp^2)^{1/2} \quad \text{for} \quad b_{C_p} = 0.008 \text{ (typical)}$$

$$b_{C_f} = [9.00\times10^{-4}\,C_f^2 + 8.47\times10^{-10} + 2.46\times10^{-5}\,C_f^2$$

$$+ 7.67\times10^{-1}\,\Delta Cp^{-2}\,C_f^2\,(1.28\times10^{-4} + 2.50\times10^{-3}\,\Delta Cp^2)]^{1/2}$$

$$= [8.47\times10^{-10} + 2.84\times10^{-3}\,C_f^2 + 1.83\times10^{-9}\,C_f^{-0.283}]^{1/2}$$

The bias error for C_f is a function of C_f itself. At low values of C_f for which the change in pressure coefficient ΔC_p is small, the bias error of C_p dominates the overall error because it becomes large with respect to the value of ΔC_p. At higher values of C_f, the error is dominated by the combined errors of block misalignment to the flow and inaccuracies of the Preston tubes. The bias error for C_f is plotted in Figure 8.

The statistical error in measuring C_f arises from the same errors in measuring ΔC_p. The error in measuring ΔCp is the square root of two times the statistical error of one C_p measurement.

$$S_{C_f} = \frac{\partial C_f}{\partial \Delta C_p} S_{\Delta C_p}$$

for which

$$S_{\Delta C_p} = \sqrt{2}\, S_{C_p}$$

$$S_{C_f} = 0.876\,\Delta C_p^{-1}\,C_f\,(6.34\times10^{-4})$$

$$= 2.39\times10^{-6}\,C_f^{-0.142}$$

and the precision error is mildly dependent on the value for C_f itself. The precision error is also plotted in Figure 8.

The bias and precision errors are combined and plotted in Figure 9 to yield the 95% confidence interval for the friction coefficient.

To minimize the error in small values of C_f, the errors in measuring C_p must be minimized primarily by checking the alignment of the pitot tubes and monitoring the pressure system during testing for thermal drift effects. These procedures should be

followed during testing to minimize the uncertainty in the coefficient, C_p. At higher friction coefficient values which result from larger differences in measured pressures, the minimum uncertainty becomes limited by the published accuracy estimates of the calibrating Preston tubes and small misalignments of the blocks to the flow.

CONCLUSIONS

An error analysis similar to the method of Abernathy [1] can be applied to determine the accuracy of the pressure and friction coefficients measured for the DARPA SUBOFF program.

The major sources of error in the pressure measurements are misalignment of the reference pitot tubes and temperature drift in the electronics. The pitot tube readings are compared during testing to check for misalignment and thermal drift in the electronics is compensated by repeated calibrations at the elevated temperatures. Over an estimated tunnel temperature rise of 7°C maximum, the true pressure coefficients will be within +0.01 and –0.0085 of the measured value. The pressure coefficient for the model nose will be within +0.013 and –0.012 of the measured value.

The greatest error sources in measuring the friction coefficients are, for small coefficient values, measuring the small difference between two pressure coefficients, and for larger friction coefficients, accuracy limits of the published calibrations for Preston tubes and flow misalignment effects. The precautions exercised for minimizing pressure coefficient errors during testing will also minimize the errors in the friction coefficients. Overall, the true friction coefficients are within ±0.0002 of their measured values.

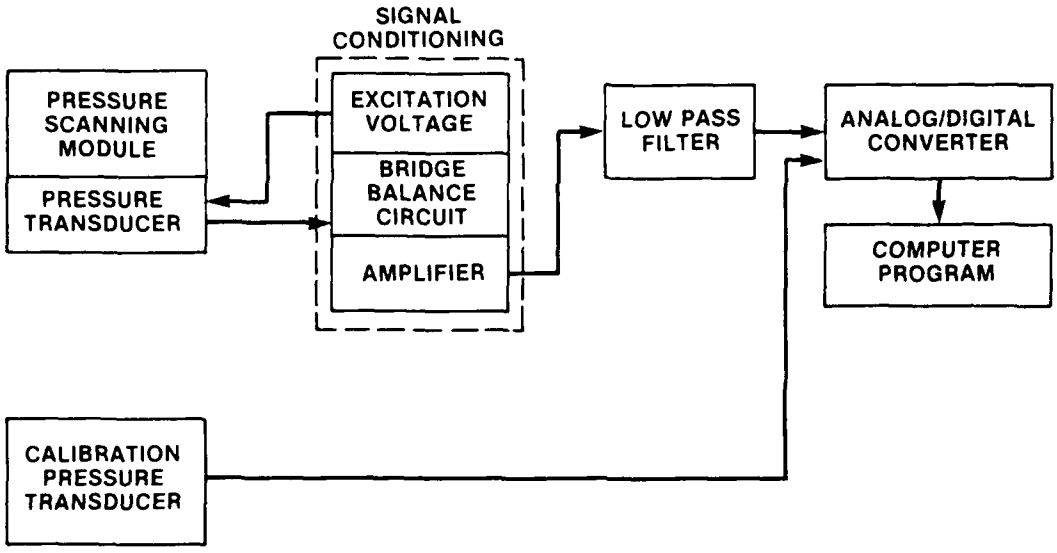

Fig. 1 Pressure system electronics

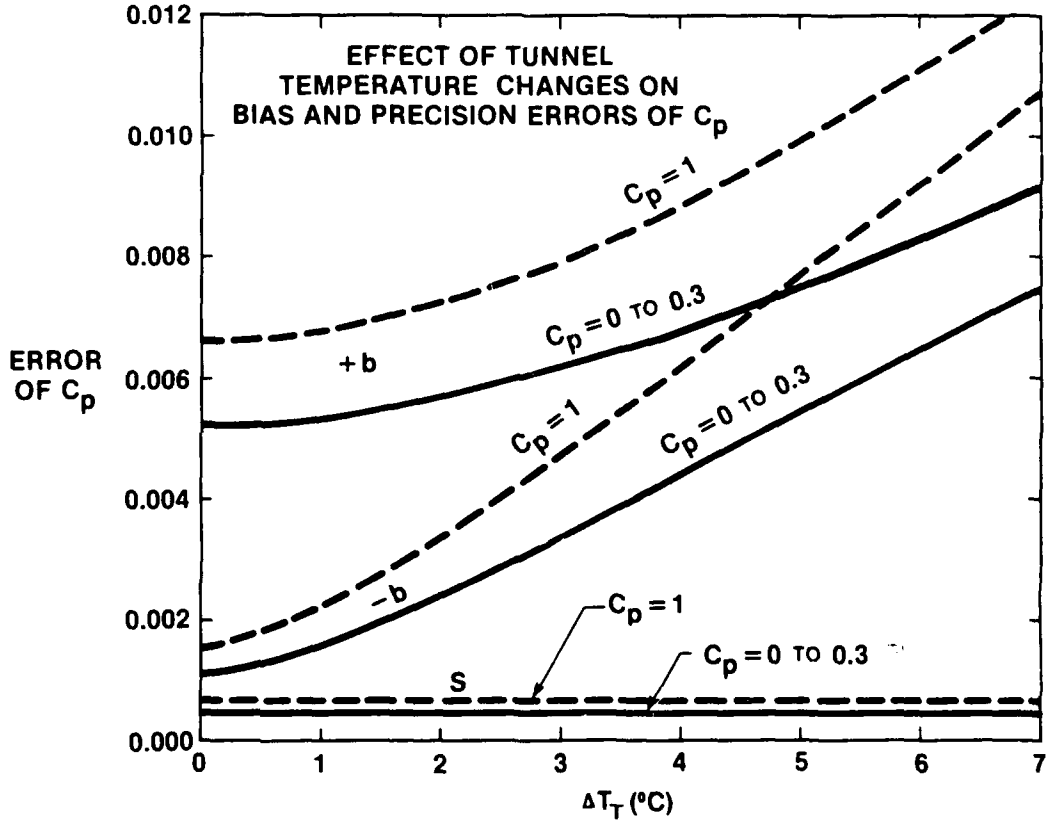

Fig. 2 Effect of tunnel temperature changes on bias and precision errors of Cp.

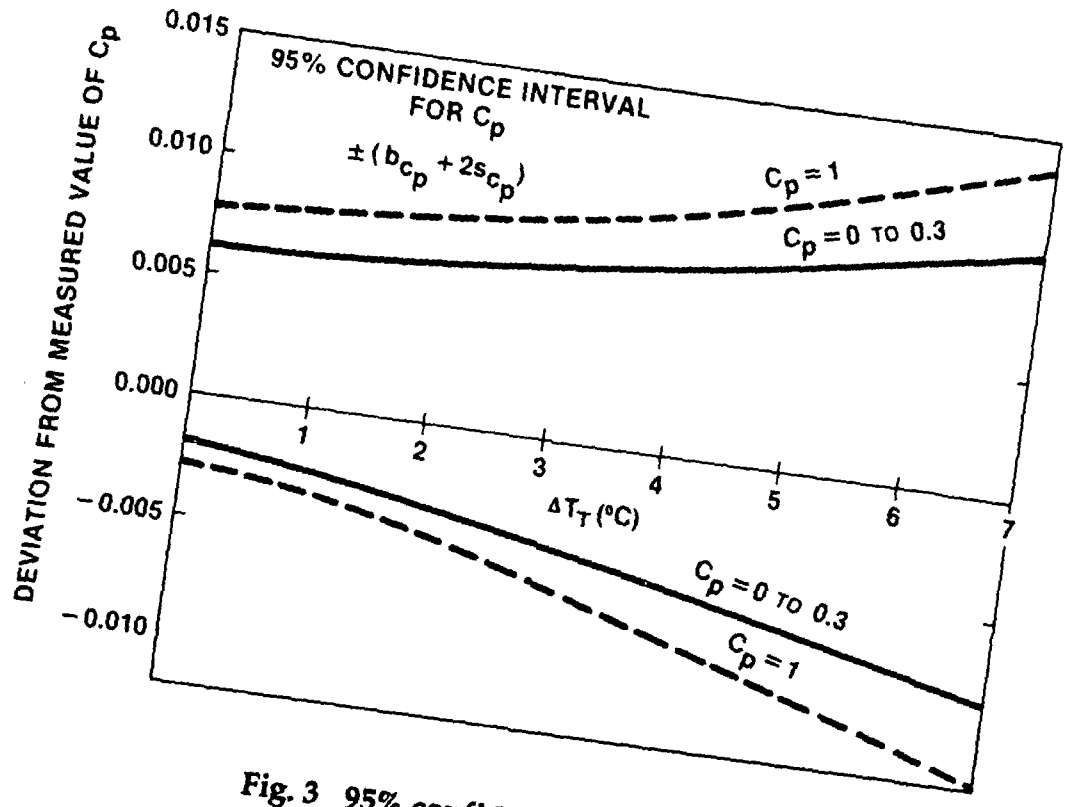

Fig. 3 95% confidence interval for C_p.

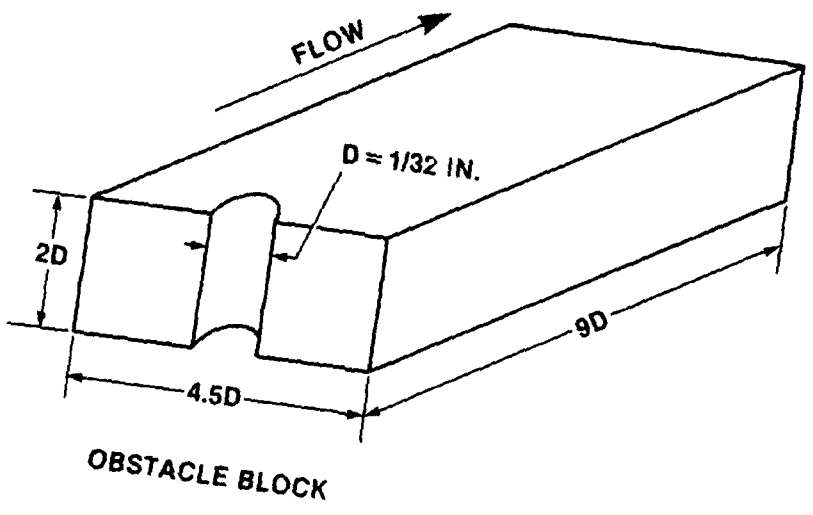

Fig. 4. Obstacle block.

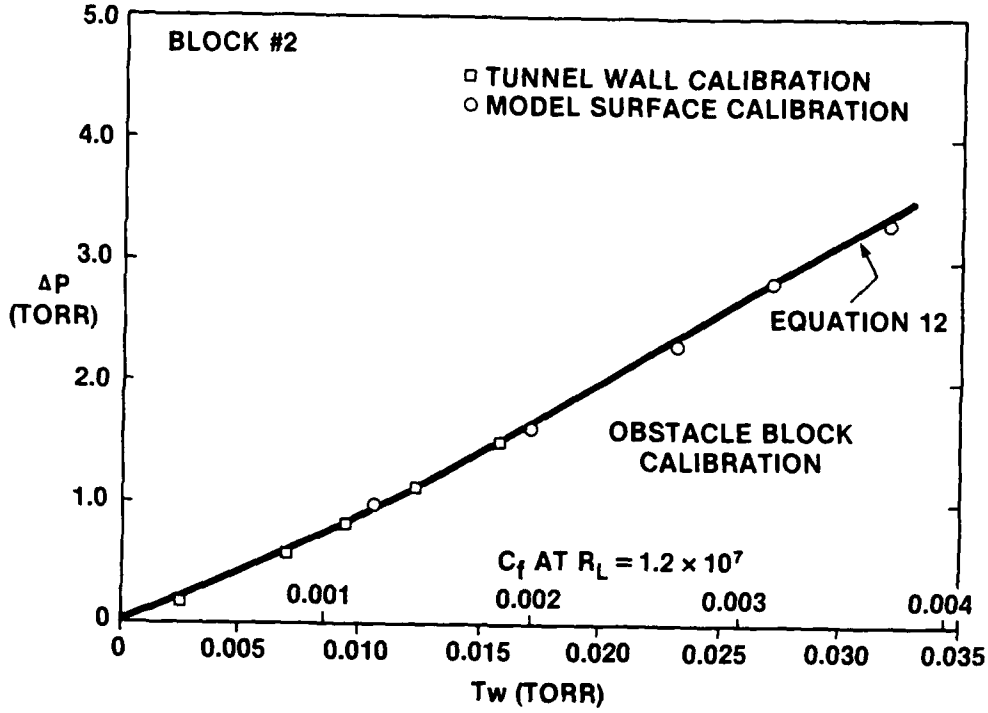

Fig. 5 Obstacle block calibration.

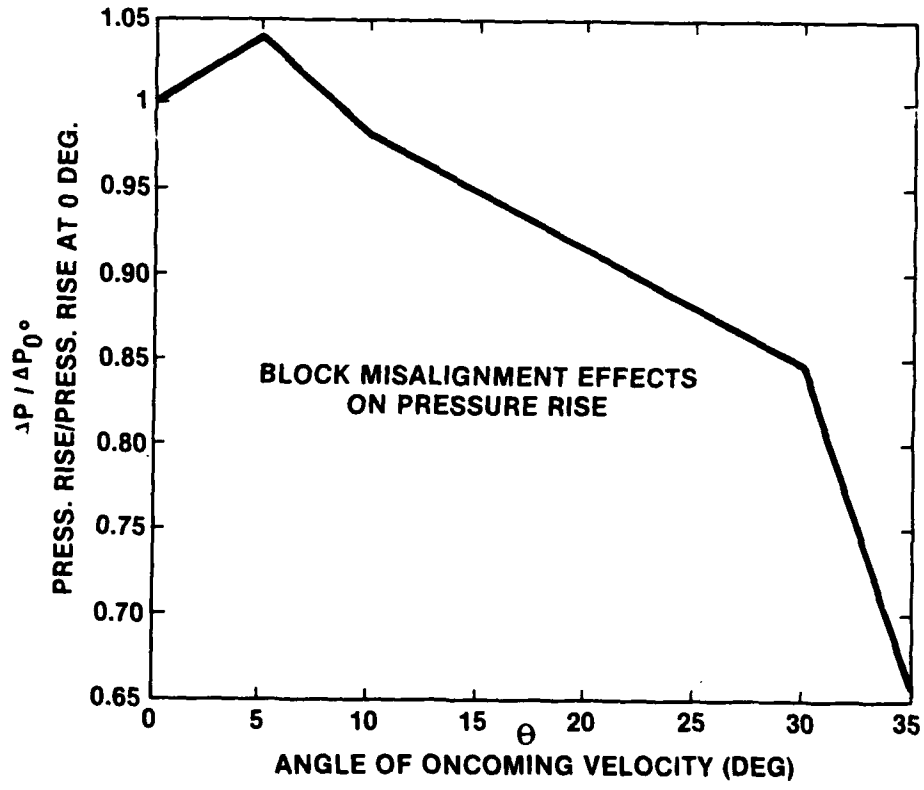

Fig. 6 Block misalignment effects on pressure rise.

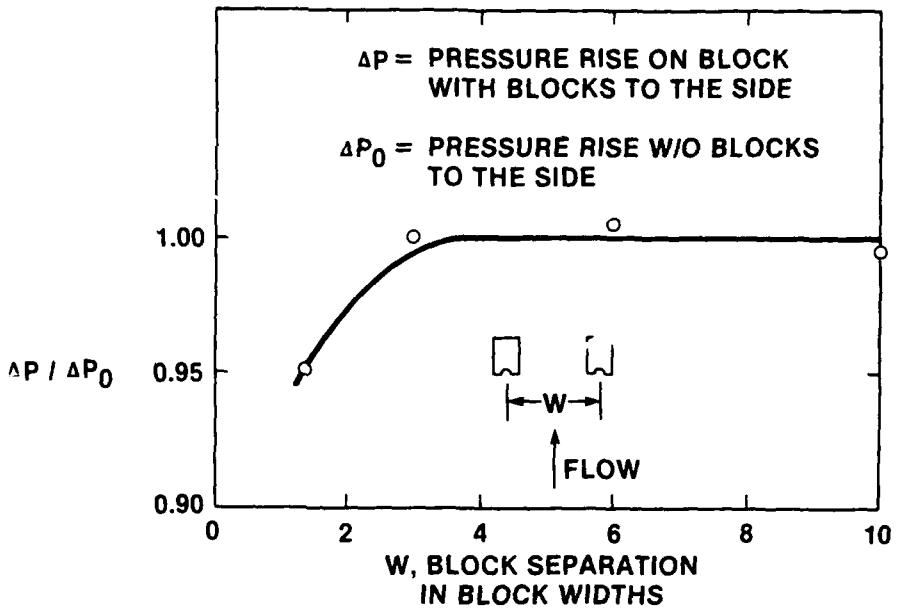

Fig. 7. Block proximity effects on pressure rise.

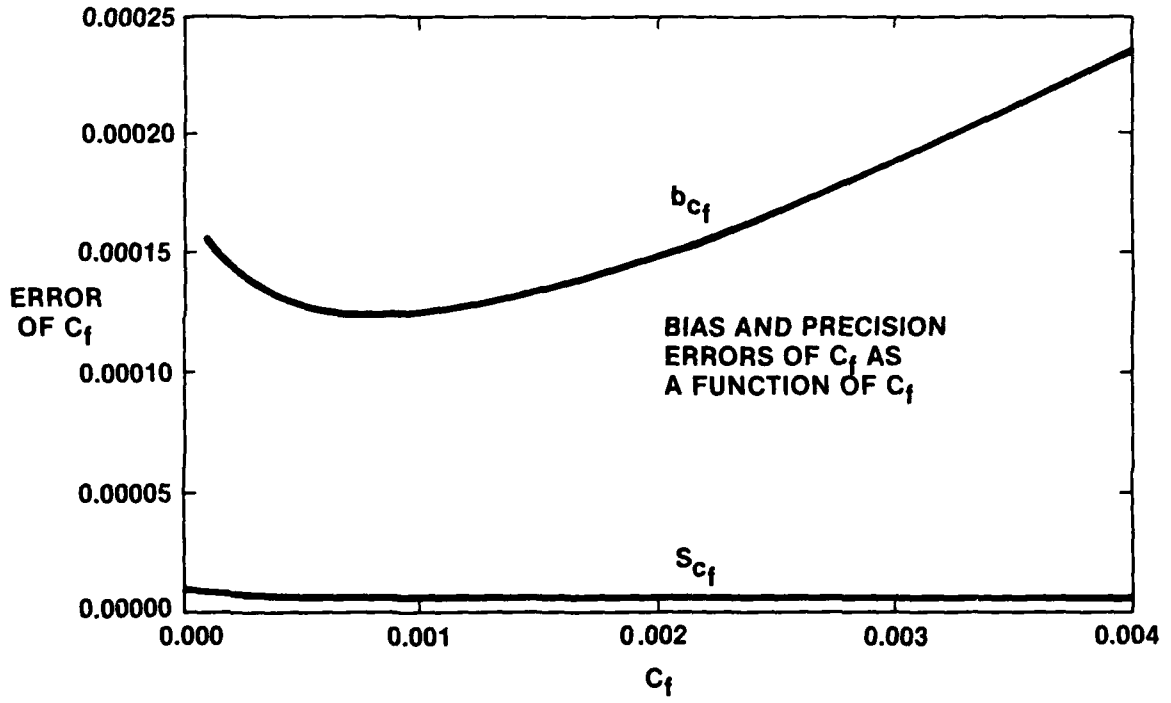

Fig. 8 Bias and precision errors of C_f as a function of C_f.

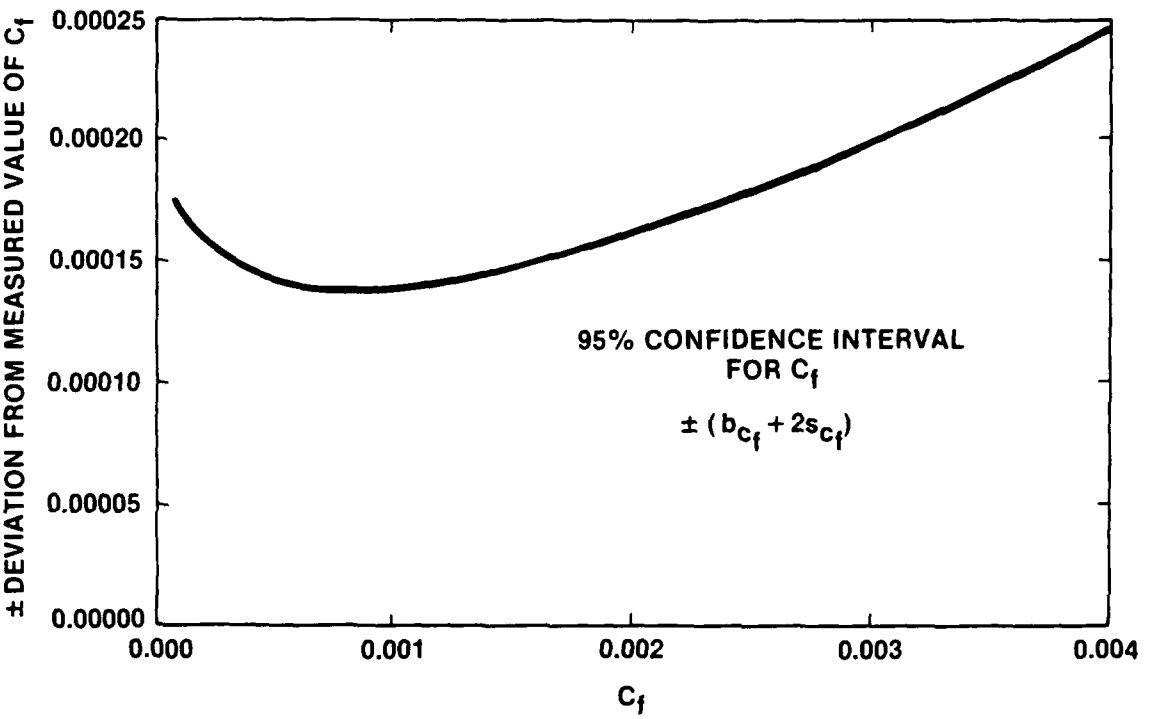

Fig. 9 95% confidence interval for C_f.

REFERENCES

1. Abernathy, R.B., et al. and Thompson, J.W. Jr., "Handbook - Uncertainty in Gas Turbine Measurements," Report No. AEDC-TR-73-5, Engine Test Facility, Arnold Engineering Development Center, Arnold Air Force Station, Tenn. (February 1973).

2. Lipson, C. and S. Narendra, *Statistical Design and Analysis of Engineering Experiments*, McGraw-Hill Book Co., New York (1973).

3. Elfstrom, G.M., "Indirect Measurement of Turbulent Skin Friction," reprinted from DME/NAE Quarterly Bulletin No. 1979, Ottawa, Canada (April 1979).

4. Winter, K.G., "An Outline of the Techniques Available for the Measurement of Skin Friction in Turbulent Boundary Layers," Prog. Aerospace Science, Vol. 18, pp. 1-57 (1977).